Coexistence of Uniform and Oscillatory States Resulting from Nonreciprocity and Conservation Laws

Daniel Greve,[1,*] Giorgio Lovato,[2,†] Tobias Frohoff-Hülsmann,[1,‡] and Uwe Thiele[1,3,4,§]
[1]Institut für Theoretische Physik, Universität Münster, Wilhelm-Klemm-Strasse 9, 48149 Münster, Germany
[2]Institut für Theoretische Physik und Astrophysik, Christian-Albrechts-Universität zu Kiel, Leibnizstrasse 5, 24098 Kiel,Germany
[3]Center for Nonlinear Science (CeNoS), Universität Münster, Corrensstrasse 2, 48149 Münster, Germany
[4]Center for Multiscale Theory and Computation (CMTC), Universität Münster, Corrensstrasse 40, 48149 Münster,Germany

(Received 14 February 2024; revised 19 June 2024; accepted 21 November 2024; published 8 January 2025)

Employing a two-species Cahn-Hilliard model with nonreciprocal interactions, we show that the interplay of nonreciprocity and conservation laws results in the robust coexistence of uniform stationary and oscillatory phases as well as of uniform and crystalline phases. For nonequilibrium models with a spurious gradient dynamics structure, such coexistences between two or more nonequilibrium phases and resulting phase diagrams can, nevertheless, be predicted by a Maxwell double-tangent construction. This includes phases with sustained regular or irregular out-of-equilibrium dynamics as further corroborated by bifurcation studies and time simulations.

DOI: 10.1103/PhysRevLett.134.018303

Thermodynamic out-of-equilibrium processes like phase separation are often described by gradient dynamics models, i.e., with continuum theories for the overdamped time evolution of densitylike order parameter fields. The existence of an underlying thermodynamic potential results in a monotonic relaxation toward an equilibrium state. Mass conservation may imply that different phases coexist in extensive parameter ranges, e.g., for a decomposing mixture as described by the classical Cahn-Hilliard (CH) model [1]. In the thermodynamic limit, the coexisting phases are predicted by a common-tangent Maxwell construction [2].

Recently, active mixtures that remain permanently out of equilibrium, e.g., due to an underlying chemomechanical coupling, have gained much attention. Descriptions by continuum theories arise from coarse-graining the dynamics of active particles [3–5], as phenomenological models [6–8], and as amplitude equations [9–11]. Examples like active model B (AMB) [12–14] and the nonreciprocal Cahn-Hilliard (NRCH) model [6–8,15] correspond to nonvariational generalizations of CH models. Thereby, AMB arises for motility-induced phase separation [4], while NRCH models describe active ternary or higher-order mixtures. Furthermore, the latter capture universal large-scale oscillatory dynamics for systems with two conservation laws [9]. Remarkably, for the single-species AMB case, a Maxwell-like construction predicts coexisting densities even though the system is nonvariational [12,16].

Here, we explain why, for an entire third class of multispecies models between classic passive (thermodynamic) ones and fully active ones, generalized Maxwell-type constructions predict nonequilibrium phase diagrams in the thermodynamic limit. We show that this is a further consequence of their spurious gradient dynamics form as introduced in Ref. [17] to explain the unexpected existence of steady asymmetric states in several common nonvariational models. This third class contains, e.g., selected active phase-field-crystal (aPFC) [18,19] and NRCH models. In consequence, for the entire model class, one can even capture the behavior of nonequilibrium phases that exist only due to activity. Figures 1(a)–1(d) illustrate the predicted coexistence of uniform and oscillatory states and of uniform and crystalline states, respectively [20]. Figure 1(a) gives a large-scale impression of two-phase coexistence where an oscillatory phase shows irregular waves, while Fig. 1(b) illustrates the sequence of regular and irregular wave patterns at small sizes of the oscillatory patch (cf. Movies 1 and 2 in Supplemental Material [21]). Figure 1(c) showcases that even three-phase coexistence of two uniform and one oscillatory phase can be predicted by the Maxwell construction.

Here, the Maxwell construction for spurious gradient dynamics models and the resulting phase behavior is illustrated employing the linearly coupled two-species NRCH model [8]

$$\partial_t u_i = \vec{\nabla} \cdot \left[Q_i \vec{\nabla} \left(\frac{\delta \mathcal{F}}{\delta u_i} + \mu_i^{\mathrm{nr}} \right) \right]. \tag{1}$$

For $i = 1, 2$, the two conservation laws describe a mixture of nonreciprocally interacting species of densities $u_1(\vec{x}, t)$

*Contact author: daniel.greve@uni-muenster.de
†Contact author: stu242274@mail.uni-kiel.de
‡Contact author: t_froh01@uni-muenster.de
§Contact author: u.thiele@uni-muenster.de; http://www.uwethiele.de

 © 2025 American Physical Society

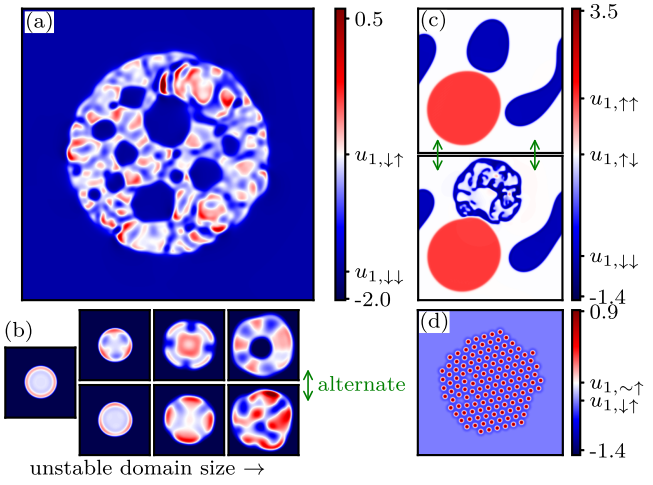

FIG. 1. Predicted phase coexistences in active phase decomposition [NRCH model (1)]. (a) Displays a snapshot of the density u_1 for the coexistence of a central cluster of an oscillatory phase with irregular wave dynamics about the high-density state $u_{1,\downarrow\uparrow}$ and a uniform low-density state $u_{1,\downarrow\downarrow}$ (blue). (b) Illustrates the transition from (left) a steady state to (middle) regular and (right) irregular wave dynamics with increasing size of the central domain for otherwise identical parameters as in (a). (c) Shows three-phase coexistence (red/blue/white) using two snapshots that illustrate (top) a "calm" period and (bottom) one of the occasional burst of wave activity in the $\downarrow\downarrow$ phase (blue). (d) Shows a central cluster of a stationary crystalline phase that coexists with a uniform phase ($u_{1,\downarrow\uparrow}$). Coexisting (mean) densities in (a, b), (c) and (d) are marked by square symbols in Figs. 2(b)–2(d), respectively. The parameters are (a)–(d) $a = -1.5$, $\rho = 1$, (a), (b) $\zeta = 3$, $\kappa = 1$, (c) $\zeta = 0.69$, $\kappa = 1$, and (d) $\zeta = 8$, $\kappa = 20$. The domain size in (a), (c), and (d) is $80\pi \times 80\pi$ and in (b) $30\pi \times 30\pi$ (only $15\pi \times 15\pi$ is shown). For numeric details and accompanying movies, see Supplemental Material [21].

and $u_2(\vec{x}, t)$, where the nonequilibrium chemical potentials are $\mu_1^{\rm nr} = -\alpha u_2$ and $\mu_2^{\rm nr} = +\alpha u_1$. The underlying energy is $\mathcal{F} = \mathcal{F}_1[u_1] + \mathcal{F}_2[u_2] + \mathcal{F}_{12}[u_1, u_2]$ with $\mathcal{F}_{12} = \int_\Omega f_{12} \mathrm{d}^n x$ where $f_{12} = -\rho u_1 u_2$, and $\mathcal{F}_i = \int_\Omega [(\kappa_i/2) |\vec{\nabla} u_i|^2 + f_i] \mathrm{d}^n x$ where $f_i = (a_i/2)u_i^2 + (b_i/4)u_i^4$. The two Q_i represent diffusional mobilities [27]. By scaling space, time, and fields, we set b_1, b_2, κ_1, and Q_1 to one. Then, $\kappa = \kappa_2/\kappa_1$ represents the rigidity ratio. For simplicity, we set $a_1 = a_2 = a$ and $Q_2 = 1$, and n is the number of spatial dimensions. Reciprocal and nonreciprocal interactions are parametrized through respective symmetric (ρ) and antisymmetric (α) coupling strengths.

The nonreciprocity parameter $\xi = \alpha^2 - \rho^2$ distinguishes cases of dominant reciprocal ($\xi < 0$) and dominant nonreciprocal ($\xi > 0$) coupling. For purely reciprocal coupling ($\alpha = 0$), Eq. (1) represent a proper gradient dynamics; see [8,28–31].

The nonreciprocal interaction breaks Newton's third law, similar to a predator-prey attraction-repulsion interaction. As a result, for dominant nonreciprocity ($\xi > 0$), the NRCH model features conserved-Hopf and -Turing instabilities [9,32], suppression of coarsening [8], localized patterns [33], sustained traveling and standing waves [7,8,34,35], and more complex spatiotemporal patterns [6,8] that are all not possible in passive CH models. The conserved-Hopf instability results in large-scale oscillatory behavior as in the central clusters in Figs. 1(a) and 1(c). The conserved-Turing instability occurs only for unequal rigidities ($\kappa \neq 1$) [32] and gives rise to small-scale stationary patterns; see Fig. 1(d). Dispersion relations and spinodals are determined in Sec. S2 in Supplemental Material [21].

At first sight, one might assume that only in the passive case ($\alpha = 0$) can coexisting states (binodals) be obtained via a common-tangent Maxwell construction. However, for Eq. (1), this holds even for dominant nonreciprocal coupling ($\xi > 0$). Specifically, introducing the spurious energy $\tilde{\mathcal{F}} = [\rho/(\rho + \alpha)]\mathcal{F}_1 + [\rho/(\rho - \alpha)]\mathcal{F}_2 + \mathcal{F}_{12}$ and mobilities $\tilde{M}_1 = [(\rho + \alpha)/\rho]$ and $\tilde{M}_2 = [(\rho - \alpha)/\rho]$, Eq. (1) can be written as a *spurious gradient dynamics*. It is spurious as for $\xi > 0$ the energy $\tilde{\mathcal{F}}$ is not bounded from below and the mobilities $\tilde{M}_i$ are not both positive; i.e., basic thermodynamic principles are not fulfilled any more. Nevertheless, as we show next, a resulting *spurious Maxwell construction* allows us to obtain coexisting states, i.e., binodals and tie lines, from a double-tangent construction on $\tilde{\mathcal{F}}$. These have to be carefully scrutinized, as in the nonreciprocal case the binodals represent only part of the picture. Taken in combination with linear stability results, the spurious Maxwell construction allows us to obtain nonequilibrium phase diagrams that, e.g., predict the coexistences in Fig. 1.

Note that the resulting phase diagram features the spinodals and binodals for all uniform and crystalline phases. For two coexisting uniform phases A and B, the double-tangent construction corresponds to the conditions $\tilde{\mu}_1(\boldsymbol{u}^{(A)}) = \tilde{\mu}_1(\boldsymbol{u}^{(B)})$, $\tilde{\mu}_2(\boldsymbol{u}^{(A)}) = \tilde{\mu}_2(\boldsymbol{u}^{(B)})$, and $\tilde{p}(\boldsymbol{u}^{(A)}) = \tilde{p}(\boldsymbol{u}^{(B)})$, where $\boldsymbol{u}^{(A)}$ and $\boldsymbol{u}^{(B)}$ are the respective densities, the spurious chemical potentials are $\tilde{\mu}_i = \partial \tilde{f}/\partial u_i$ with $\tilde{f} = [\rho/(\rho + \alpha)]f_1 + [\rho/(\rho - \alpha)]f_2 + f_{12}$, and the spurious pressure is $\tilde{p} = \tilde{\mu}_1 u_1 + \tilde{\mu}_2 u_2 - \tilde{f}$. The generalization for cases involving crystalline phases is provided in Sec. S1 in Supplemental Material [21].

Resulting phase diagrams are given in Fig. 2. The reciprocal reference case in Fig. 2(a) features four uniform phases (with high and low densities u_i as indicated by the arrows in the four corners) and allows for five two- and two three-phase coexistences. Nonreciprocity results in various changes in the phase behavior [Figs. 2(b)–2(d)]: Because $\alpha \neq 0$, Figs. 2(b)–2(d) do not show the field exchange symmetry ($u_1 \leftrightarrow u_2$) of Fig. 2(a); however, field inversion $[(u_1, u_2) \leftrightarrow (-u_1, -u_2)]$ is retained. Only the outer regions where at least one $|\bar{u}_i|$ is large, are qualitatively as in Fig. 2(a), as the reciprocal nonlinear parts of the f_i dominate. Changes due to nonreciprocity are strongest in

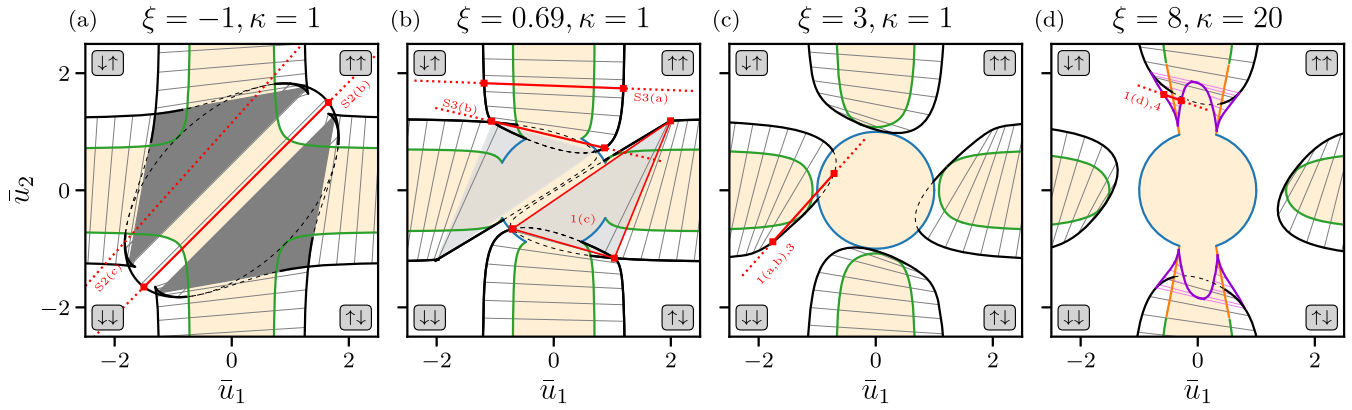

FIG. 2. Phase diagrams in the $(\bar{u}_1, \bar{u}_2)$ plane for the NRCH model for increasing nonreciprocity $\xi = \alpha^2 - \rho^2$ (left to right) at (a)–(c) unity ($\kappa = 1$) and (d) nonunity ($\kappa = 20$) rigidity ratio. For coexisting uniform phases, solid thick black and thin gray lines represent (stable and metastable) binodals and tie lines, respectively. Purple lines in (d) represent binodals for coexisting uniform and crystalline phases (tie lines are pink). Dashed black lines indicate unstable binodals; i.e., the coexisting state is unstable. The dark [light] gray area in (a) [(b)] marks stable [unstable] three-phase coexistence. The white areas in the four corners are single-phase regions, e.g., top left of the ↓↑ phase (low u_1, high u_2). Green, orange, and blue lines indicate spinodals for Cahn-Hilliard, conserved-Turing, and (oscillatory) conserved-Hopf instabilities, respectively. Remaining parameters are $\rho = 1$ and $a = -1.5$. For red straight lines, see the main text.

the central region of low $|\bar{u}_i|$. In Fig. 2(b) ($\xi = 0.69$), the three-phase coexistence has become unstable, as the coexisting phase of lowest $|\bar{u}_i|$ has crossed the threshold of the oscillatory instability. Furthermore, the stable coexistence of ↓↓ and ↑↑ phases has disappeared. Example bifurcation structures and density profiles along the highlighted red tie lines in Figs. 2(a) and 2(b) are discussed in Secs. S3 and S4 in Supplemental Material [21], respectively.

At larger nonreciprocity [$\xi = 3$, Fig. 2(c)], the four pairs of binodals have entirely separated, triple-point regions and ↓↓-↑↑ coexistence have disappeared, and the Hopf threshold now forms a closed curve that, most importantly, intersects some binodals. In other words, part of the coexisting states are oscillatory unstable, thereby predicting the coexistence of a uniform state and an oscillatory state of different mean densities. This effectively predicts the behavior found in Figs. 1(a) and 1(b) and can be further appreciated in the dramatically changed bifurcation structure; see Fig. 3(a). There, branches of steady states are analyzed as one follows the red tie line in Fig. 2(c), where the binodal at small $|\bar{u}_i|$ corresponds to a Hopf-unstable ↓↑ state. At the spinodals, a branch of steady phase-separated

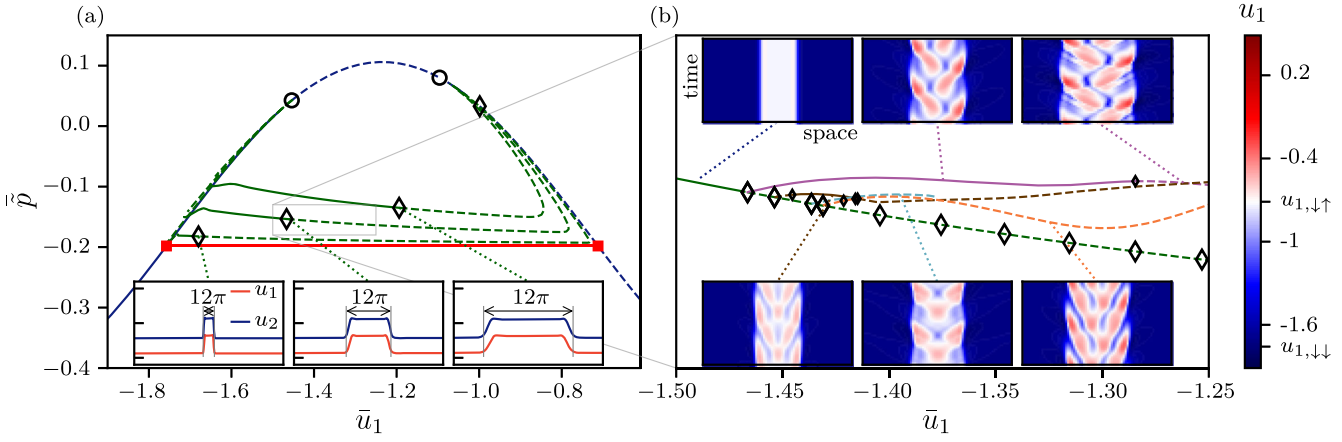

FIG. 3. (a) Bifurcation diagram giving the (mean) pressure $\bar{\tilde{p}}$ over $\bar{u}_1$ along the red tie line in the phase diagram Fig. 2(c) [$\bar{u}_2 = 1.116\bar{u}_1 + 1.081$]. Branches of uniform and phase-separated states are given as blue and green lines, respectively. For the latter, curves are given for three domain sizes $L = 20\pi$, 40π, and 160π (top to bottom). The red line and squares indicate the Maxwell construction in the thermodynamic limit. Insets give the profiles at the Hopf bifurcations on the three branches. (b) Magnification of the branch of stationary phase-separated states for $L = 40\pi$ including more Hopf bifurcations than (a) and the first emerging branches of time-periodic states. The insets show space-time plots of different states where patches of oscillatory states coexist with the uniform steady background state. Solid [dashed] lines indicate linearly stable [unstable] states. Circles [diamonds] mark Cahn-Hilliard [Hopf] instabilities. Small diamonds in (b) indicate torus bifurcations, i.e., Hopf bifurcations of oscillatory states.

states (green, shown for three domain sizes L) emerges from the branch of uniform states (blue) and undergoes saddle-node bifurcations (on the left and on the right). For large domains, the almost horizontal central part approaches the red Maxwell line. However, in stark contrast to Figs. S2 and S3 in Supplemental Material [21], here, when increasing $\bar{u}_1$ the steady phase-separated state becomes oscillatory unstable at a Hopf bifurcation. For all considered L, this occurs when the unstable $\downarrow\uparrow$ phase has grown to a critical size $\ell_c \approx 12\pi$ [insets in Fig. 3(a)] [36].

The magnification in Fig. 3(b) shows that more such bifurcations follow and result in the emergence of several branches of time-periodic states. Intriguingly, these indeed correspond to the stable coexistence of a uniform $\downarrow\downarrow$ phase with an oscillatory $\downarrow\uparrow$ phase with domain sizes defined by the lever rule [branch in Fig. 3(b) that bifurcates supercritically at $\bar{u}_1 \approx -1.47$ and eventually destabilizes at a torus bifurcation]. Corresponding time simulations in 1D (see Sec. S4 in Supplemental Material [21]) confirm the prediction of Fig. 3. The robustness of the predicted uniform-oscillatory coexistence is further evidenced by the 2D case already presented in Fig. 1(a). Interestingly, large domains of the irregular oscillatory state tend to split (in 1D) or develop inner holes filled by the uniform phase (in 2D). Although this might seem similar to the "bubbly phase separation" observed for AMB+ in 2D [13], close inspection reveals that here the holes evolve very slowly and do practically not fuse with each other or with the domain interface [37]. If the oscillatory domain is sufficiently small, three-, four-, or fivefold waves are observed, the latter circling a periodically appearing self-organized ring structure around a central hole [Fig. 1(b) and Movie 1(b) in Supplemental Material [21]]. Furthermore, Fig. 2(b) even predicts three-phase coexistence of two stable uniform phases with a weakly unstable oscillatory one. This is indeed found in Fig. 1(c), where the blue unstable phase shows irregular bursts of waves interspersed with long "calm" phases.

Focusing next on the phase diagram in Fig. 2(d), we see that further increasing the nonreciprocity ξ separates the binodals from the Hopf-unstable region. In contrast to the previous cases, Fig. 2(d) features a conserved-Turing instability (case of nonunity rigidity ratio, $\kappa \neq 1$) giving rise to crystalline phases. The resulting (purple) binodals represent their coexistence with uniform phases; see the magnification in Fig. 4(a). With increasing $|\bar{u}_2|$, the lattice spacing of the crystalline states increases and finally diverges at $(\bar{u}_1, \bar{u}_2) \approx (0, 1.9)$ (not shown). In other words, the crystalline phase transforms into a phase-separated state with a smooth transition between the binodals. In contrast, when decreasing $|\bar{u}_2|$, the coexistence ranges shrink till they terminate in tricritical points where the phase transition changes from first to second order. Figures 4(b) and 4(c) show the bifurcation structure along the red tie line in

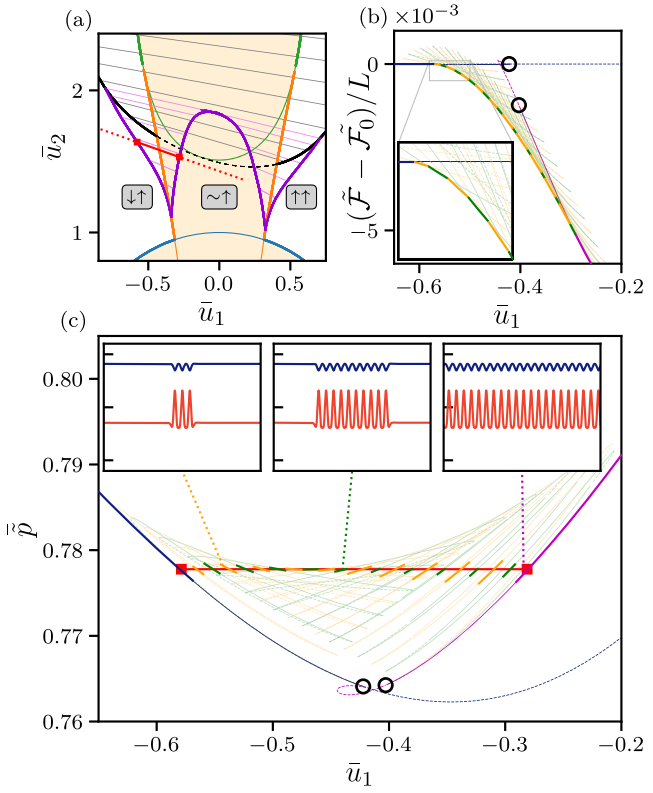

FIG. 4. (a) Magnifies part of Fig. 2(d) focusing on the coexistence region of uniform and crystalline phases. (b),(c) Analyze the bifurcation structure along the red tie line in (a) [$\bar{u}_2 = -0.353\bar{u}_1 + 1.431$] providing mean energy and pressure $\bar{\tilde{p}}$ over $\bar{u}_1$, respectively. Shown are uniform (blue), periodic (magenta), and even [odd] (green [yellow]) localized states, i.e., crystallites. (b),(c) Highlight the states of lowest energy as piecewise thick lines, thereby in (c) illustrating how the Maxwell line (red horizontal) is approached. Parameters are as in Fig. 4(d) and $L = 80\pi$.

Fig. 4(a) in terms of mean energy and pressure, respectively. Where the uniform state (stable at small $\bar{u}_1$) undergoes the conserved-Turing instability, a branch of periodic (crystalline) states emerges, itself soon spawning two branches of localized states forming the typical "snakes and ladders" structure [38–40]. The ensuing multistability represents phase coexistence: The heavy lines in Figs. 4(b) and 4(c) highlight respective states of minimal spurious energy $\tilde{\mathcal{F}}$. Also see the example of a 2D crystallite in Fig. 1(d). In this way, Fig. 4(c) reveals that the resulting piecewise curve defines a narrow horizontal band centered about the coexistence pressure. With increasing domain size, the band will become thinner and approach the Maxwell line as known from the passive PFC model [41]. The validity of the approach of [41] for the studied NRCH model impressively evidences the power of the spurious gradient dynamics form.

In conclusion, we have shown that several aspects of the equilibrium thermodynamics of phase transitions can be

applied to a third class of models between passive and active systems that features a spurious gradient dynamics structure. In particular, employing a specific NRCH model, we have illustrated that the resulting (spurious) Maxwell construction allows one to predict its phase behavior, intriguingly, including the nonequilibrium two- and three-phase coexistence of uniform and oscillatory states featuring large-amplitude regular or irregular waves. We expect such coexistences to widely occur in systems with conservation laws that show large-scale oscillatory instabilities [9,32,42]; see, e.g., [43,44]. Notably, this includes crystalline (or microphase-separated) states that also emerge only due to nonreciprocity. Extending the calculation of spurious pressure and chemical potential to crystalline phases (see Supplemental Material [21]), we have further shown that the full characterization of first-order phase transitions via bifurcation diagrams developed for PFC models [41] applies in the present nonequilibrium case.

Our analysis of the specific NRCH model already indicates the validity of the approach for all models in the class of spurious gradient dynamics, like active PFC models [18,19,45], coupled Cahn-Hilliard and Swift-Hohenberg models [17], and the FitzHugh-Nagumo RD model [46,47]. All of these could be (re)investigated defining corresponding nonequilibrium chemical potentials $\tilde{\mu}_i$ and pressures $\tilde{p}$ as described in Supplemental Material [21] which, in turn, can be combined with extensions of mechanistic views of microscopic systems [49,50]. Resulting nonequilibrium multispecies coexistence conditions, e.g., [51,52], may then be further unified and employed to further elucidate the interplay of conservation laws and nonreciprocity.

[1] J. W. Cahn and J. E. Hilliard, Free energy of a nonuniform system. 3. Nucleation in a 2-component incompressible fluid, J. Chem. Phys. **31**, 688 (1959).

[2] J. Clerk-Maxwell, On the dynamical evidence of the molecular constitution of bodies, Nature (London) **11**, 357 (1875).

[3] A. Dinelli, J. O'Byrne, A. Curatolo, Y. Zhao, P. Sollich, and J. Tailleur, Non-reciprocity across scales in active mixtures, Nat. Commun. **14**, 7035 (2023).

[4] M. E. Cates and J. Tailleur, Motility-induced phase separation, Annu. Rev. Condens. Matter Phys. **6**, 219 (2015).

[5] M. te Vrugt, J. Bickmann, and R. Wittkowski, How to derive a predictive field theory for active Brownian particles: A step-by-step tutorial, J. Phys. Condens. Matter **35**, 313001 (2023).

[6] S. Saha, J. Agudo-Canalejo, and R. Golestanian, Scalar active mixtures: The non-reciprocal Cahn-Hilliard model, Phys. Rev. X **10**, 041009 (2020).

[7] Z. H. You, A. Baskaran, and M. C. Marchetti, Nonreciprocity as a generic route to traveling states, Proc. Natl. Acad. Sci. U.S.A. **117**, 19767 (2020).

[8] T. Frohoff-Hülsmann, J. Wrembel, and U. Thiele, Suppression of coarsening and emergence of oscillatory behavior in a Cahn-Hilliard model with nonvariational coupling, Phys. Rev. E **103**, 042602 (2021).

[9] T. Frohoff-Hülsmann and U. Thiele, Nonreciprocal Cahn-Hilliard model emerges as a universal amplitude equation, Phys. Rev. Lett. **131**, 107201 (2023).

[10] F. Bergmann, L. Rapp, and W. Zimmermann, Active phase separation: A universal approach, Phys. Rev. E **98**, 020603 (R) (2018).

[11] L. Rapp, F. Bergmann, and W. Zimmermann, Systematic extension of the Cahn-Hilliard model for motility-induced phase separation, Eur. Phys. J. E **42**, 57 (2019).

[12] R. Wittkowski, A. Tiribocchi, J. Stenhammar, R. J. Allen, D. Marenduzzo, and M. E. Cates, Scalar ϕ^4 field theory for active-particle phase separation, Nat. Commun. **5**, 4351 (2014).

[13] E. Tjhung, C. Nardini, and M. E. Cates, Cluster phases and bubbly phase separation in active fluids: Reversal of the Ostwald process, Phys. Rev. X **8**, 031080 (2018).

[14] J. Bickmann and R. Wittkowski, Collective dynamics of active Brownian particles in three spatial dimensions: A predictive field theory, Phys. Rev. Res. **2**, 033241 (2020).

[15] T. Suchanek, K. Kroy, and S. A. M. Loos, Irreversible mesoscale fluctuations herald the emergence of dynamical phases, Phys. Rev. Lett. **131**, 258302 (2023).

[16] A. P. Solon, J. Stenhammar, M. E. Cates, Y. Kafri, and J. Tailleur, Generalized thermodynamics of phase equilibria in scalar active matter, Phys. Rev. E **97**, 020602(R) (2018).

[17] T. Frohoff-Hülsmann, M. P. Holl, E. Knobloch, S. V. Gurevich, and U. Thiele, Stationary broken parity states in active matter models, Phys. Rev. E **107**, 064210 (2023).

[18] A. M. Menzel and H. Löwen, Traveling and resting crystals in active systems, Phys. Rev. Lett. **110**, 055702 (2013).

[19] L. Ophaus, S. V. Gurevich, and U. Thiele, Resting and traveling localized states in an active phase-field-crystal model, Phys. Rev. E **98**, 022608 (2018).

[20] Because of their analogy to PFC structures, we refer to crystal-like periodic microphase-separation structures as "crystalline" and to corresponding localized states as "crystallites".

[21] See Supplemental Material at http://link.aps.org/supplemental/10.1103/PhysRevLett.134.018303 which includes Refs. [22–26] for additional information and details on the numerical methods used.

[22] M. P. Holl, A. J. Archer, and U. Thiele, Efficient calculation of phase coexistence and phase diagrams: Application to a binary phase-field crystal model, J. Phys. Condens. Matter **33**, 115401 (2021).

[23] A. M. Turing, The chemical basis of morphogenesis, Phil. Trans. R. Soc. B **237**, 37 (1952).

[24] H. Uecker, D. Wetzel, and J. D. M. Rademacher, pde2path —a Matlab package for continuation and bifurcation in 2D elliptic systems, Numer. Math. Theory Methods Appl. **7**, 58 (2014).

[25] H. Uecker, Hopf bifurcation and time periodic orbits with pde2path-algorithms and applications, Commun. Comput. Phys. **25**, 812 (2019).

[26] D. Greve, G. Lovato, T. Frohoff-Hülsmann, and U. Thiele, Data supplement for "Coexistence of uniform and

oscillatory states resulting from nonreciprocity and conservation laws," 10.5281/zenodo.14236238 (2024).
[27] Cross-diffusion and dependence on u_1 and u_2 are neglected, as no change in our main argument would result.
[28] J. W. Cahn and J. E. Hilliard, Free energy of a nonuniform system. 1. Interfacial free energy, J. Chem. Phys. **28**, 258 (1958).
[29] J. W. Cahn, Phase separation by spinodal decomposition in isotropic systems, J. Chem. Phys. **42**, 93 (1965).
[30] P. C. Hohenberg and B. I. Halperin, Theory of dynamic critical phenomena, Rev. Mod. Phys. **49**, 435 (1977).
[31] A. J. Bray, Theory of phase-ordering kinetics, Adv. Phys. **43**, 357 (1994).
[32] T. Frohoff-Hülsmann, U. Thiele, and L. M. Pismen, Nonreciprocity induces resonances in a two-field Cahn-Hilliard model, Phil. Trans. R. Soc. A **381**, 20220087 (2023).
[33] T. Frohoff-Hülsmann and U. Thiele, Localised states in coupled Cahn-Hilliard equations, IMA J. Appl. Math. **86**, 924 (2021).
[34] T. Suchanek, K. Kroy, and S. A. M. Loos, Entropy production in the nonreciprocal Cahn-Hilliard model, Phys. Rev. E **108**, 064610 (2023).
[35] F. Brauns and M. C. Marchetti, Nonreciprocal pattern formation of conserved fields, Phys. Rev. X **14**, 021014 (2024).
[36] The observed ℓ_c is approximately 4 times larger than the smallest unstable wavelength that results from the linear stability analysis of a uniform state of the $\downarrow\uparrow$ phase. However, here we observe that the oscillation extends across the phase boundary into the linearly stable $\downarrow\downarrow$-phase, where it propagates as a traveling wave with exponentially damped amplitude. Because of this damping, the first self-sustained oscillation occurs at larger domains and with larger critical wavelengths compared to the standing waves emerging from an isolated uniform $\downarrow\uparrow$-state with, e.g., Neumann boundary condition.
[37] Furthermore, in contrast to [13], no additional noise is needed to create or sustain them.
[38] J. Burke and E. Knobloch, Localized states in the generalized Swift-Hohenberg equation, Phys. Rev. E **73**, 056211 (2006).
[39] E. Knobloch, Localized structures and front propagation in systems with a conservation law, IMA J. Appl. Math. **81**, 457 (2016).
[40] M. P. Holl, A. J. Archer, S. V. Gurevich, E. Knobloch, L. Ophaus, and U. Thiele, Localized states in passive and active phase-field-crystal models, IMA J. Appl. Math. **86**, 896 (2021).
[41] U. Thiele, T. Frohoff-Hülsmann, S. Engelnkemper, E. Knobloch, and A. J. Archer, First order phase transitions and the thermodynamic limit, New J. Phys. **21**, 123021 (2019).
[42] D. Greve and U. Thiele, An amplitude equation for the conserved-Hopf bifurcation – derivation, analysis, and assessment, Chaos **34**, 123134 (2024).
[43] N. B. Padhan and R. Pandit, Activity-induced droplet propulsion and multifractality, Phys. Rev. Res. **5**, L032013 (2023).
[44] Y. Duan, J. Agudo-Canalejo, R. Golestanian, and B. Mahault, Dynamical pattern formation without self-attraction in quorum-sensing active matter: The interplay between nonreciprocity and motility, Phys. Rev. Lett. **131**, 148301 (2023).
[45] M. te Vrugt, M. P. Holl, A. Koch, R. Wittkowski, and U. Thiele, Derivation and analysis of a phase field crystal model for a mixture of active and passive particles, Model. Simul. Mater. Sci. Eng. **30**, 084001 (2022).
[46] P. Schütz, M. Bode, and H. G. Purwins, Bifurcations of front dynamics in a reaction-diffusion system with spatial inhomogeneities, Physica (Amsterdam) **82D**, 382 (1995).
[47] Here, the list comprises models with purely mass-conserving, purely non-mass-conserving, and mixed dynamics. Note that further generalizations of the spurious gradient structure will surely exist as other similar structures have been described that only partially overlap with the form introduced in [17]. This includes the skew-gradient dissipative systems of [48]; cf. discussion in conclusion of [17], the Maxwell-like construction in [16], see Sec. S5 of Supplemental Material [21], and the mechanistic discussion of coexistence in [49].
[48] M. Kuwamura and E. Yanagida, The Eckhaus and zigzag instability criteria in gradient/skew-gradient dissipative systems, Physica (Amsterdam) **175D**, 185 (2003).
[49] A. K. Omar, H. Row, S. A. Mallory, and J. F. Brady, Mechanical theory of nonequilibrium coexistence and motility-induced phase separation, Proc. Natl. Acad. Sci. U.S.A. **120**, e2219900120 (2023).
[50] A. V. Ivlev, J. Bartnick, M. Heinen, C.-R. Du, V. Nosenko, and H. Löwen, Statistical mechanics where Newton's third law is broken, Phys. Rev. X **5**, 011035 (2015).
[51] Y.-J. Chiu, D. Evans, and A. K. Omar, Theory of nonequilibrium multicomponent coexistence, arXiv:2409.07620.
[52] A. Dinelli, Scalar active matter across scales, Ph.D. thesis, Paris, 2024, https://theses.hal.science/tel-04708958v1.